

# Understanding Mass Transfer Directions via Data-Driven Models with Application to Mobile Phone Data

Alessandro Alla

*Departamento de Matemática, PUC-Rio, Rio de Janeiro, Brazil*

Caterina Balzotti

*Dipartimento di Scienze di Base e Applicate per l'Ingegneria, Sapienza Università di Roma,  
Rome, Italy*

Maya Briani and Emiliano Cristiani

*Istituto per le Applicazioni del Calcolo "M. Picone", Consiglio Nazionale delle Ricerche,  
Rome, Italy*

---

## Abstract

The aim of this paper is to solve an inverse problem which regards a mass moving in a bounded domain. We assume that the mass moves following an unknown velocity field and that the evolution of the mass density can be described by partial differential equations (PDEs), which is also unknown. The input data of the problems are given by some snapshots of the mass distribution at certain times, while the sought output is the velocity field that drives the mass along its displacement. To this aim, we put in place an algorithm based on the combination of two methods: first, we use the Dynamic Mode Decomposition to create a mathematical model describing the mass transfer; second, we use the notion of Wasserstein distance (also known as earth mover's distance) to reconstruct the underlying velocity field that is responsible for the displacement. Finally, we consider a real-life application: the algorithm is employed to study the travel flows of people in large populated areas using, as input data, density profiles (i.e. the spatial distribution) of people in given areas at different time instances. This kind of data are provided by the Italian telecommunication company TIM and are derived by mobile phone usage.

*Keywords:* Data-driven methods, dynamic mode decomposition, Wasserstein distance, earth mover’s distance, cellular data, presence data.

*2010 MSC:* 37C10, 35R30, 76D55.

---

## 1. Introduction

In this paper we aim at solving an inverse problem which regards a mass moving in a bounded domain with finite velocity. We assume that the mass moves following an unknown velocity field and that the evolution of the mass density can be described by an unknown PDE. The input data of the problem are given by some snapshots of the mass distribution at certain times, while the sought information is the velocity field that drives the mass along its displacement.

The basic idea can be summarized as follows: given two snapshots of the mass distribution at two instants of time, we want to understand where each portion of the mass (which is assumed to be conserved from one instant of time to the other) is transported from/to, i.e. how the first spatial distribution is rearranged in the second one. The goal is pursued by computing a numerical approximation of the Wasserstein distance (also known as earth mover’s distance or Mallows distance) between the two consecutive density profiles, specifying a suitable cost function which measures the “energy” consumed by the system for moving forward. The computation of the Wasserstein distance gives, as a by-product, the minimum-cost mass flow from the first to the second configuration, i.e. how the mass distributes in space and time.

Despite the good preliminary results obtained by the above described Wasserstein-based approach [2, 18], the algorithm is found to be excessively expensive both in terms of CPU time and memory requirements. This fact strongly restricts the applicability of the method. To fix this, in this paper we propose to couple the method with the Dynamic Mode Decomposition (DMD): a data-driven technique that takes in input the snapshots of the mass distribution and returns an analytical approximation of the dynamics underlying the mass trans-

fer. More precisely, it provides a system of ODEs which describes the evolution of the mass in any point of the domain. Solving the ODEs, we are able to recover the mass distribution *at any time*, thus increasing at will the number of available snapshots or, analogously, decreasing at will the time frame between them. Controlling the time frame between two consecutive snapshots is the key to simplify the computation of the Wasserstein distance and makes the computation of the flows feasible even on large domains.

Finally, a real-world application of the proposed methodology is illustrated. We are interested in inferring activity-based human mobility flows from mobile phone data. We assume that mobile devices are not singularly tracked, but their logs are aggregated in order to obtain the total number of users in a given area. In this way we get the density profiles (i.e. the spatial distribution) of people in a given area at various instants of time. The dataset we have at our disposal is provided by the Italian telecommunication company TIM. The time frame between two consecutive snapshots is 15 minutes.

As before, the goal is to “assign a direction” to the presence data. In fact, the mere representation of time varying density of people clearly differentiate attractive from repulsive or neutral areas but does not provide any information about the directions of flows of people. In other words, we are interested in a “where-from-where-to” type of information, which reveals travel flows and patterns of people providing a sort of *origin-destination* matrix.

*Paper organization..* The paper is organized as follows. In Section 2 we present the DMD method and the Wasserstein distance. In Section 3 we show how to couple those method to obtain an efficient algorithm. In Section 4 we apply the proposed approach to real-life data. Finally in Section 5 we draw our conclusions.

## 2. Mathematical background

In this section we recall the building blocks of the methodology proposed in the paper, namely the DMD method used to build a data-driven model, and the

Wasserstein distance to determine the transport map driving the moving mass.

### 2.1. DMD method

DMD is a data-driven method capable of providing accurate assessments of the spatio-temporal coherent structures in a given complex system, or short-time future estimates of such a systems. Although a complete list of references for DMD goes beyond the scopes of this work, we would like to mention [3, 5, 6, 12, 14]. In the current work we use the DMD algorithm as in [15].

To begin, we suppose to have a set of data  $\mathcal{X} = \{\mathbf{y}(t_0), \dots, \mathbf{y}(t_{n_t})\}$  for some time instances  $\{t_j\}_{j=0}^{n_t}$  with  $\mathbf{y}(t_j) \in \mathbb{R}^n, j = 0, \dots, n_t$ . The goal of the method is to build a mathematical model upon the dataset  $\mathcal{X} \in \mathbb{R}^{n \times (n_t+1)}$ . The DMD procedure thus constructs the approximate linear evolution  $\tilde{\mathbf{y}}(t)$  for the dataset  $\mathcal{X}$  exploiting its low-rank structure:

$$\frac{d\tilde{\mathbf{y}}}{dt} = \mathbf{A}\tilde{\mathbf{y}} \quad (2.1)$$

where  $\mathbf{A} \in \mathbb{R}^{n \times n}$  is unknown,  $\tilde{\mathbf{y}}(0) = \tilde{\mathbf{y}}_0$ , and the solution has the form

$$\tilde{\mathbf{y}}(t) = \sum_{i=1}^r \beta_i \psi_i \exp(\omega_i t), \quad (2.2)$$

where  $r < n$ ,  $\psi_i$  and  $\omega_i$  are the eigenfunctions and eigenvalues of the unknown matrix  $\mathbf{A}$ . The coefficients  $\beta_i$  of the vector  $\boldsymbol{\beta}$  can be determined from the initial data. For example, at  $t = t_0$  we have  $\mathbf{y}(t_0) = \mathbf{y}_0$  so that (2.2) gives  $\boldsymbol{\beta} = \boldsymbol{\Psi}^\dagger \mathbf{y}_0$  where  $\boldsymbol{\Psi}$  is a matrix comprised of the DMD modes  $\psi_i$  and  $\dagger$  denotes the Moore-Penrose pseudo-inverse. To compute the matrix  $\mathbf{A}$ , we first split the dataset into two snapshot matrices

$$\mathbf{Y} = \begin{bmatrix} | & | & & | \\ \mathbf{y}(t_0) & \mathbf{y}(t_1) & \cdots & \mathbf{y}(t_{n_t-1}) \\ | & | & & | \end{bmatrix}, \quad \mathbf{Y}' = \begin{bmatrix} | & | & & | \\ \mathbf{y}(t_1) & \mathbf{y}(t_2) & \cdots & \mathbf{y}(t_{n_t}) \\ | & | & & | \end{bmatrix} \quad (2.3)$$

and suppose the following linear relation hold true:

$$\mathbf{Y}' = \mathbf{A}\mathbf{Y}. \quad (2.4)$$



Specifically, we assume that  $\mathbf{y}(t_j)$  is an initial condition to obtain  $\mathbf{y}(t_{j+1})$ , i.e. its corresponding output after some prescribed evolution time  $\Delta t > 0$ . Thus, the DMD method computes the best linear operator  $\mathbf{A}$  relating to the matrices above:

$$\mathbf{A} = \mathbf{Y}'\mathbf{Y}^\dagger. \quad (2.5)$$

We refer to  $\mathbf{Y}$  and  $\mathbf{Y}'$  as input and output snapshot matrices respectively.

Clearly, the DMD algorithm aims at optimally constructing the matrix  $\mathbf{A}$  so that the error between the true and approximate solution is small in a least-square sense, i.e.  $\|\mathbf{y}(t) - \tilde{\mathbf{y}}(t)\| \ll 1$ . Of course, the optimality of the approximation holds only over the sampling window where  $\mathbf{A}$  is constructed, but the approximate solution can be used to not only make future state predictions, but also to decompose the dynamics into various time-scales, since the method computes eigenvalues and eigenvectors of the matrix  $\mathbf{A}$ .

In practice, the matrix  $\mathbf{A}$  is, in general, highly ill-conditioned and when the state dimension  $n$  is large, the aforementioned matrix may be even intractable to analyze directly. Instead, DMD circumvents the eigen-decomposition of  $\mathbf{A}$  by considering a low rank representation in terms of a POD-projected matrix  $\tilde{\mathbf{A}}$ . Although the description of the POD method goes beyond the scopes of this paper, we recall that the POD projection solves the following optimization problem

$$\min_{\varphi_1, \dots, \varphi_r \in \mathbb{R}^n} \sum_{j=1}^{n_t} \left\| \mathbf{y}(t_j) - \sum_{i=1}^r \langle \mathbf{y}(t_j), \varphi_i \rangle \varphi_i \right\|^2 \quad \text{such that } \langle \varphi_i, \varphi_j \rangle = \delta_{ij}, \quad (2.6)$$

where  $\{\varphi_i\}_{i=1}^r$  are the POD projectors. The solution of the optimization problem (2.6) is obtained by means of a Singular Value Decomposition (SVD) of the data set  $\mathcal{X}$ , where the first  $r \ll n$  columns of the left singular eigenvectors are the required POD basis. We refer to [17] for a complete description of the POD method. We also mention that POD method is equivalent to Principal Component Analysis (PCA) or Karhunen-Lo  ve expansion in other context (see e.g. [8, 9]).

The exact DMD algorithm proceeds as follows [15]: First, we collect data  $\mathbf{Y}, \mathbf{Y}'$  as in (2.3) and compute the reduced, or economy, singular value decomposition of  $\mathbf{Y}$ :

$$\mathbf{Y} = \mathbf{U}\mathbf{\Sigma}\mathbf{V}^T.$$

We note that the use of the economy SVD is suggested since the matrices  $\mathbf{Y}, \mathbf{Y}' \in \mathbb{R}^{n \times n_t}$  with  $n \gg n_t$  and that the economy  $\mathbf{U} \in \mathbb{R}^{n \times r}$  is sufficient to provide the same approximation of the regular SVD given the limited amount of snapshots.

Furthermore, the DMD typically makes use of low-rank structure so that the total number of modes,  $r \ll n$ , allows for dimensionality reduction of the dynamical system. Then, we compute the least-squares fit  $\mathbf{A}$  that satisfies  $\mathbf{Y}' = \mathbf{A}\mathbf{Y}$  and project onto the POD modes  $\mathbf{U}$ . Specifically, the Moore-Penrose pseudo-inverse of  $\mathbf{Y}$  allows us to compute  $\mathbf{A} = \mathbf{Y}'\mathbf{Y}^\dagger$ , where the Moore-Penrose algorithm provides the least-square fitting procedure. In terms of its low-rank projection, this yields:

$$\tilde{\mathbf{A}} = \mathbf{U}^T \mathbf{A} \mathbf{U} = \mathbf{U}^T \mathbf{Y}' \mathbf{V} \mathbf{\Sigma}^{-1},$$

and compute the eigen-decomposition of  $\tilde{\mathbf{A}} \in \mathbb{R}^{r \times r}$ :

$$\tilde{\mathbf{A}} \mathbf{W} = \mathbf{W} \mathbf{\Lambda},$$

where  $\mathbf{\Lambda}$  are the DMD eigenvalues. Finally, the DMD modes  $\mathbf{\Psi}^{\text{DMD}}$  are given by:

$$\mathbf{\Psi}^{\text{DMD}} = \mathbf{Y}' \mathbf{V} \mathbf{\Sigma}^{-1} \mathbf{W}. \quad (2.7)$$

The algorithm is summarized in **Algorithm 1**.

---

**Algorithm 1** Exact DMD

---

**Require:** Snapshots  $\{\mathbf{y}(t_0), \dots, \mathbf{y}(t_{n_t})\}$ ,

- 1: Set  $\mathbf{Y} = [\mathbf{y}(t_0), \dots, \mathbf{y}(t_{n_t-1})]$  and  $\mathbf{Y}' = [\mathbf{y}(t_1), \dots, \mathbf{y}(t_{n_t})]$ .
  - 2: Compute the reduced SVD of rank  $r$  of  $\mathbf{Y}$ ,  $\mathbf{Y} = \mathbf{U}\mathbf{\Sigma}\mathbf{V}^T$ .
  - 3: Define  $\tilde{\mathbf{A}} := \mathbf{U}^T \mathbf{Y}' \mathbf{V} \mathbf{\Sigma}^{-1}$ .
  - 4: Compute eigenvalues and eigenvectors of  $\tilde{\mathbf{A}} \mathbf{W} = \mathbf{W} \mathbf{\Lambda}$ .
  - 5: Set  $\mathbf{\Psi}^{\text{DMD}} = \mathbf{Y}' \mathbf{V} \mathbf{\Sigma}^{-1} \mathbf{W}$ .
-

## 2.2. Wasserstein distance

The notion of Wasserstein distance is strictly related to the Monge–Kantorovich optimal mass transfer problem [16], which can be easily explained as follows: given a sandpile with mass distribution  $\rho^i$  and a pit with equal volume and mass distribution  $\rho^f$ , find a way to minimize the cost of transporting sand into the pit. The cost for moving mass depends on both the distance from the point of origin to the point of arrival and the amount of mass is moved along that path. We are interested in minimizing this cost by finding the optimal path to transport the mass from the initial to the final configuration.

Given two density functions  $\rho^i, \rho^f : \Omega \rightarrow \mathbb{R}$  for some bounded  $\Omega \subset \mathbb{R}^n$ , we define the  $L^p$ -Wasserstein distance between  $\rho^i$  and  $\rho^f$  as

$$W_p(\rho^i, \rho^f) = \left( \min_{T \in \mathcal{T}} \int_{\Omega} c(\boldsymbol{\xi}, T(\boldsymbol{\xi}))^p \rho^i(\boldsymbol{\xi}) d\boldsymbol{\xi} \right)^{\frac{1}{p}} \quad (2.8)$$

where

$$\mathcal{T} := \left\{ T : \Omega \rightarrow \Omega : \int_B \rho^f(\boldsymbol{\xi}) d\boldsymbol{\xi} = \int_{\{\boldsymbol{\xi} : T(\boldsymbol{\xi}) \in B\}} \rho^i(\boldsymbol{\xi}) d\boldsymbol{\xi}, \quad \forall B \subset \Omega \right\}$$

and  $c : \Omega \times \Omega \rightarrow \mathbb{R}$  is a given cost function, which defines the cost of transferring a unit mass between any two points in  $\Omega$ . Note that  $\mathcal{T}$  is the set of all possible maps which transfer the mass from one configuration to the other.

It is important to note here that we are not really interested in the actual value of the Wasserstein distance  $W_p$ , instead we look for the *optimal map*  $T^*$  which realizes the argmin in (2.8), and represents the paths along which the mass is transferred.

## 2.3. Numerical approximation of the Wasserstein distance

A direct numerical approximation of definition (2.8) is unfeasible, but a discrete approach is still possible. Indeed, we can resort to classical problems (see Hitchcock’s paper [7]) and methods (see e.g., [11, Sec. 6.4.1] and [13, Chap. 19]) to recast the original mass transfer problem in the framework of linear programming (LP). We also refer to [4] for a recent application of this methodology to traffic flow problems.

The idea consists in approximating the set  $\Omega$  with a structured grid with  $N$  square cells  $C_1, \dots, C_N$ , as it is commonly done for the numerical approximation of PDEs. We denote by  $\Delta x$  the length of each side of the cells. Then, we define a graph  $\mathcal{G}$  whose nodes coincide with the centers of the  $N$  cells. Graph's edges are defined in such a way that each node is directly connected with each other, including itself.

Introducing a numerical error (controlled by the parameter  $\Delta x$ ), we are allowed to assume that  $\forall j = 1, \dots, N$  all the mass distributed in the cell  $C_j$  is concentrated in its center, i.e. in a node of the graph. We come up with an initial mass  $m_j^i := \int_{C_j} \rho^i dx$  and a final mass  $m_j^f := \int_{C_j} \rho^f dx$ , for  $j = 1, \dots, N$ , distributed on the graph nodes. Now, we simply aim at optimally rearranging the first mass into the second one moving it among the graph's nodes.

We denote by  $c_{jk}$  the cost to transfer a unit mass from node  $j$  to node  $k$ , and by  $x_{jk}$  the (unknown) mass moving from node  $j$  to node  $k$ . The problem is then formulated as

$$\text{minimize } \mathcal{H} := \sum_{j,k=1}^N c_{jk} x_{jk}$$

subject to

$$\sum_k x_{jk} = m_j^i \quad \forall j, \quad \sum_j x_{jk} = m_k^f \quad \forall k \quad \text{and} \quad x_{jk} \geq 0.$$

Defining

$$\begin{aligned} \mathbf{x} &= (x_{11}, x_{12}, \dots, x_{1N}, x_{21}, \dots, x_{2N}, \dots, x_{N1}, \dots, x_{NN})^T, \\ \mathbf{c} &= (c_{11}, c_{12}, \dots, c_{1N}, c_{21}, \dots, c_{2N}, \dots, c_{N1}, \dots, c_{NN})^T, \\ \mathbf{b} &= (m_1^i, \dots, m_N^i, m_1^f, \dots, m_N^f)^T, \end{aligned}$$

and the  $2N \times N^2$  matrix

$$\mathbf{M} = \begin{bmatrix} \mathbb{1}_N & 0 & 0 & \dots & 0 \\ 0 & \mathbb{1}_N & 0 & \dots & 0 \\ 0 & 0 & \mathbb{1}_N & \dots & 0 \\ \vdots & \vdots & \vdots & \ddots & \vdots \\ 0 & 0 & 0 & \dots & \mathbb{1}_N \\ \mathbf{I}_N & \mathbf{I}_N & \mathbf{I}_N & \mathbf{I}_N & \mathbf{I}_N \end{bmatrix},$$

where  $\mathbf{I}_N$  is the  $N \times N$  identity matrix and  $\mathbb{1}_N = \underbrace{(1 \ 1 \dots 1)}_{N \text{ times}}$ , our problem is written as a standard LP problem:

$$\begin{aligned} \min \quad & \mathbf{c}^T \mathbf{x}, \\ \text{subject to} \quad & \mathbf{M} \mathbf{x} = \mathbf{b}, \\ & \mathbf{x} \geq 0. \end{aligned} \tag{2.9}$$

The result of the algorithm is a vector  $\mathbf{x}^* := \arg \min \mathbf{c}^T \mathbf{x}$  whose elements  $x_{jk}^*$  represent how much mass moves from node  $j$  to node  $k$  employing the minimum-cost mass rearrangement.

**Remark 1.** The dimension of the LP problem (2.9) is given by the dimensions of the matrix/vectors involved:

$$\dim \mathbf{x} = \dim \mathbf{c} = N^2, \quad \dim \mathbf{b} = 2N, \quad \dim \mathbf{M} = 2N^3.$$

**Remark 2.** Hereafter we will refer to problem (2.9) as *global*, in order to stress the fact that it is possible to move the mass from and to any node of the graph.

### 3. Coupling DMD and Wasserstein distance

In this section we describe how we can drastically reduce the size of the LP problem (2.9) by using the DMD method. The resulting algorithm will allow us to study the mass transfer problem on large domains.

### 3.1. Main idea

The large size of the LP problem (2.9) mainly comes from the fact that the mass is allowed to be transferred from any graph node to any other graph node. However physical constraints prevent this to happening: assuming that the maximal velocity of the mass is  $V_{\max}$  and denoting by  $\Delta t$  the time frame from one snapshot to the following one, the maximal distance travelled is  $V_{\max}\Delta t$ . Using DMD, we are able to reconstruct the state of the system at any time and any time resolution, even much smaller than the original resolution of the dataset. Reducing the time interval between two snapshots we get a restriction on the set of all possible movements trajectories. In order to minimize the CPU time, the best choice for  $\Delta t$  is the one which guarantees that the CFL-like condition

$$V_{\max}\Delta t = \Delta x \quad (3.1)$$

holds true. In this way the *mass is allowed to move only towards the adjacent cells or not move at all*.

Under the assumption (3.1), we are allowed to simplify the LP problem (2.9), reducing its size. Let us denote by  $d$  the maximum number of neighbors per cell. The new unknown  $\tilde{x}_{jk}$ , corresponding to the mass to be moved from node  $j$  to node  $k$ , is defined only if  $j$  and  $k$  are adjacent or  $j$  is equal to  $k$ . Analogously we define the cost function  $\tilde{c}_{jk}$ . We also define the vectors  $\tilde{\mathbf{x}}$  of the unknowns and the vector  $\tilde{\mathbf{c}}$  associated to the cost function. Their elements are ordered in such a way that first we have elements related to all possible movements from node 1, then those related to movements from node 2, and so on until the  $N$ -th node. Since the mass can move only towards a maximum of  $d$  nodes, the dimensions

of  $\tilde{\mathbf{x}}$  and  $\tilde{\mathbf{c}}$  are lower or equal than  $dN$ . We introduce the matrix

$$\widetilde{\mathbf{M}} = \begin{bmatrix} \mathbb{1}_d & 0 & 0 & \dots & 0 \\ 0 & \mathbb{1}_d & 0 & \dots & 0 \\ 0 & 0 & \mathbb{1}_d & \dots & 0 \\ \vdots & \vdots & \vdots & \ddots & \vdots \\ 0 & 0 & 0 & \dots & \mathbb{1}_d \\ & & \widetilde{\mathbf{M}}_1 & & \end{bmatrix},$$

where  $\mathbb{1}_d = \underbrace{(1 \ 1 \dots 1)}_{d \text{ times}}$  and  $\widetilde{\mathbf{M}}_1$  is the adjacency matrix associated to the graph.

Defining the vector  $\tilde{\mathbf{b}} = (m_1^i, \dots, m_N^i, m_1^f, \dots, m_N^f)^T$  the LP problem becomes

$$\begin{aligned} \min \quad & \tilde{\mathbf{c}}^T \tilde{\mathbf{x}}, \\ \text{subject to} \quad & \widetilde{\mathbf{M}} \tilde{\mathbf{x}} = \tilde{\mathbf{b}} \\ & \tilde{\mathbf{x}} \geq 0. \end{aligned} \tag{3.2}$$

**Remark 3.** The dimension of the LP problem (3.2) is given by the dimensions of the matrix/vectors involved:

$$\dim \tilde{\mathbf{x}} = \dim \tilde{\mathbf{c}} \leq dN, \quad \dim \tilde{\mathbf{b}} = 2N, \quad \dim \widetilde{\mathbf{M}} \leq 2dN^2.$$

**Remark 4.** Hereafter we will refer to problem (3.2) as *local*, in order to stress the fact that it is possible to move the mass from and to adjacent nodes of the graph only.

### 3.2. An example: the DMD for the viscous Burger's equation

In this section we will include a numerical experiment using data generated by the 2D viscous Burgers's equation:

$$\begin{cases} \partial_t y - \frac{1}{100} \Delta y + y \cdot \nabla y = 0, & \mathbf{x} \in \Omega, t \in [0, T] \\ y(\mathbf{x}, t) = 0, & \mathbf{x} \in \partial\Omega \\ y(\mathbf{x}, 0) = \sin(\pi x_1) \sin(\pi x_2) & \mathbf{x} \in \Omega, \end{cases} \tag{3.3}$$

with  $\mathbf{x} = (x_1, x_2)$  and  $\Omega = [0, 1] \times [0, 1]$ . The numerical approximation of equation (3.3) has been carried out using Finite Difference method using an adaptive Runge-Kutta method for the time integration with temporal step size  $\Delta t > 0$ . The semi discrete problem has dimension  $n = 1600$ . We refer to [10] for further details on the numerical method. In what follows, since we do not know the analytical solution of equation, we consider as *exact solution* of (3.3) its numerical approximation with  $\Delta t = 0.0125$  and  $\Delta x = 0.01$ .

To show how DMD reconstructs the model we consider as data set  $\mathcal{X}$  the numerical approximation of (3.3) for the following temporal step size  $\Delta t = \{0.1, 0.05, 0.025, 0.0125\}$ . Once the snapshots have been computed we apply Algorithm 1 and reconstruct the solution corresponding with a fixed  $\delta t = 0.0125$ . Here, we aim at testing the capability of the DMD method to approximate the dataset for the missing information.

In Figure 1, we compare the exact solution of (3.3) in the top row and the absolute difference between the exact solution and the reconstructed one with DMD in the bottom row for two time instances. We note that the dataset corresponds to the solution of (3.3) with  $\Delta t = 0.1$ .

Then, in Figure 2 we show the relative error computed with respect to the Frobenius norm between the DMD approximation and the exact solution of (3.3). It is clear that the more information on the system, e.g. amount of snapshots, the better error behavior for the DMD solution. However, we can already obtain accurate solutions with a poor dataset. Finally in the right panel of Figure 2 we show the error of the model for each time instance for the dataset corresponding to  $\Delta t = \{0.1, 0.05, 0.025\}$ . We note that DMD behaves very well for time instances provided in the snapshot set. This is to show that DMD is able to reconstruct the solution for missing information and it will be crucial for the goal of our work. In this example the rank  $r$  in the DMD method is 9. Finally, we would like to emphasize that, although the DMD model is linear, it works even for nonlinear problem as, e.g., (3.3).



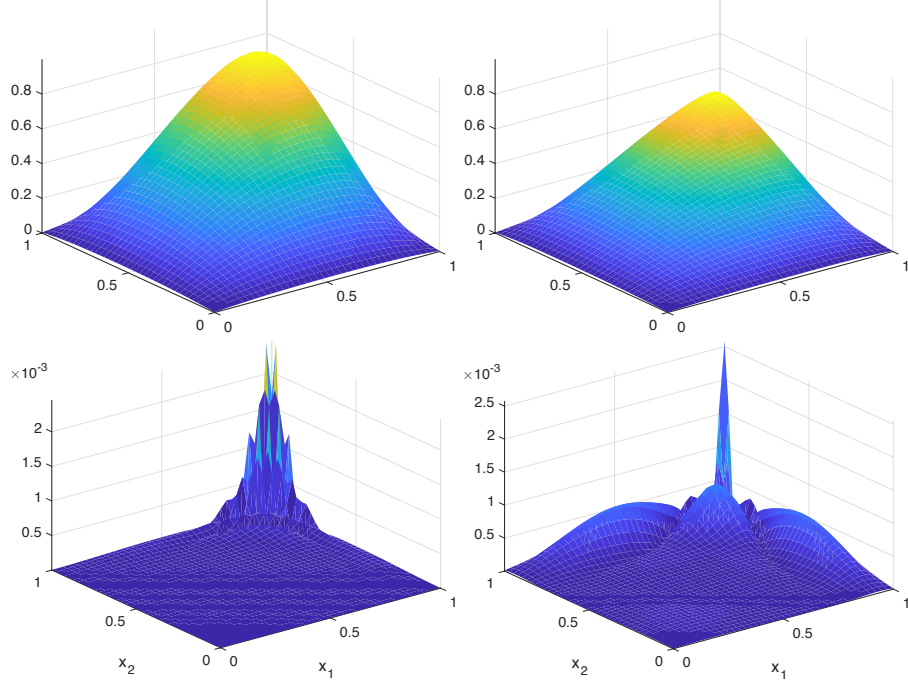


Figure 1: Top: Reference Solution for Burgers' equation at time  $t = 0.4875$  (left) and  $t = 0.9875$  (right). Bottom: absolute difference between exact solution and DMD reconstruction with data  $\Delta t = 0.1$  at time  $t = 0.4875$  (left) and  $t = 0.9875$  (right).

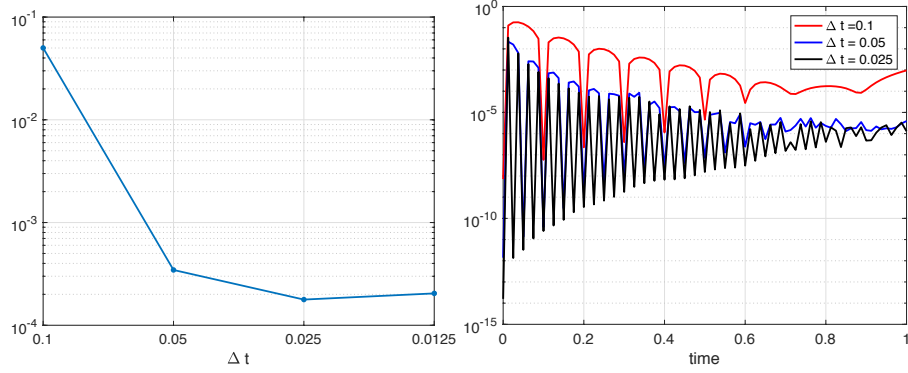


Figure 2: Error analysis of the DMD reconstruction with a reference solution computed with  $\Delta t = 0.0125$  and dataset corresponding to  $\Delta t = \{0.1, 0.05, 0.025, 0.0125\}$  as in the  $x$ -axis (left) and relative error for each time instance for the DMD reconstruction with  $\Delta t = \{0.1, 0.05, 0.025\}$  (right).

### 3.3. A toy example for the complete algorithm: the advection equation

In this test we join the two techniques described in sections 2.1 and 2.2. Let us consider the advection equation:

$$\begin{cases} \partial_t u(\mathbf{x}, t) + \mathbf{v} \cdot \nabla u(\mathbf{x}, t) = 0, & \mathbf{x} \in \Omega, t \in [0, T], \\ u(\mathbf{x}, t) = 0, & \mathbf{x} \in \partial\Omega \\ u(\mathbf{x}, 0) = u_0(\mathbf{x}), & \mathbf{x} \in \Omega, \end{cases} \quad (3.4)$$

with  $\mathbf{x} = (x_1, x_2)$ ,  $\Omega = [-2, 2] \times [-2, 2]$ ,  $u_0(\mathbf{x}) = \max(0.5 - x_1^2 - x_2^2, 0)$  and constant velocity  $\mathbf{v} = (1, 1)$ . It is well known that the analytical solution of (3.4) is  $u(\mathbf{x}, t) = u_0(\mathbf{x} - \mathbf{v}t)$  provided that we set  $T$  small enough to have inactive boundary conditions, as it is the case here.

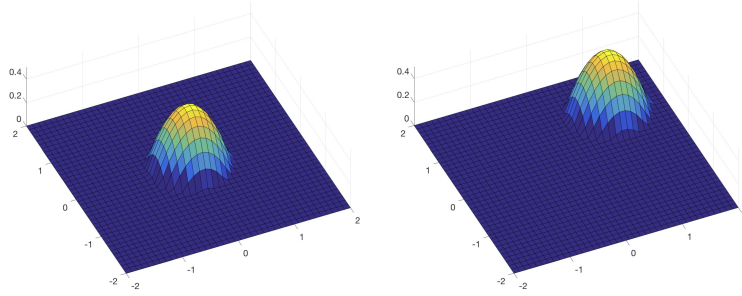


Figure 3: Exact solution of equation 3.4 at time  $t = 0$  on the left and time  $t = 2$  on the right.

Starting from some snapshots of the solution, we aim at reconstructing the velocity field driving the dynamics, i.e. the vector  $\mathbf{v} = (1, 1)$ . In doing this, we will also compare the global and the local problem in terms of CPU time, see (2.9) and (3.2) respectively.

As already done in Section 3.2, we choose a time step  $\delta t$ , and we collect snapshots with a larger temporal step size  $\Delta t = \kappa \delta t$  with  $\kappa \geq 1$  and, finally, we reconstruct the solution via the DMD method. We note that here the snapshots are computed from the analytical solution of (3.4). In particular, we work on a grid  $40 \times 40$  and we choose  $T = 2$ ,  $\Delta x = 0.1$ ,  $\delta t = 0.07$  and  $\Delta t = 2 \delta t$ . We observe that, since  $V_{max} = \sqrt{2}$ , this choice of  $\delta t$  fullfills the condition (3.1).

Moreover we identify the nodes of the graph  $\mathcal{G}$  of the numerical approximation of Wasserstein distance with the cells of the grid.

*Choice of the cost function.* Since the cost function is used to figure out the “price to pay” for moving the mass from a node of the graph to another one, the most intuitive definition of  $c$  is the Euclidean distance in  $\mathbb{R}^2$ . This choice was proved to be unsuitable for the global problem, see [2]. Indeed, since the global algorithm allows any movements between the nodes of the graph, using the Euclidean distance for the function  $c$  we loose the uniqueness of the optimal transfer map  $T^*$ . To see this let us assume that we have to move three unit masses one to the right. In the graph on the left of Figure 4 we move the three unit masses of one to the right, in the graph on the right we move only the first mass of three to the right, but the Wasserstein distance is the same and equal to three.

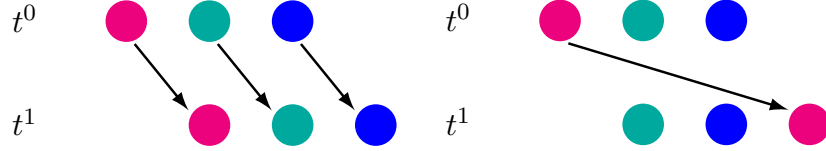


Figure 4: Three small movements on the left and one big movement on the right.

The solution proposed in [2] to fix this issue was to force the minimization algorithm to select primarily the small movements penalizing the large ones. To get this, the cost function was defined as

$$c(\xi_1, \xi_2) = \|\xi_1 - \xi_2\|_{\mathbb{R}^2}^{1+\varepsilon}, \quad (3.5)$$

where  $\xi_1$  and  $\xi_2$  are the coordinates of the nodes of the graph and  $\varepsilon > 0$  is a small parameter which accounts for the penalization.

In Figure 5 we show the level sets of the solution to (3.4) together with some arrows indicating the reconstructed velocity field  $\mathbf{v}$ . More precisely, on the top row of figure we show the results obtained with the local algorithm

(3.2), on the center with the global algorithm with Euclidean distance and on the bottom with the global algorithm with the cost function defined in (3.5) (with  $\varepsilon = 0.1$ ). Similarly, the left panels show the results obtained with the exact solution whereas the right panels those obtained with the DMD solution.

The local algorithm and the global one with the correction in (3.5) are able to reconstruct the velocity field  $\mathbf{v} = (1, 1)$  with accurate approximation. The global algorithm with Euclidean distance, instead, is less precise, since the optimal flow does not correspond to the velocity field. Moreover, the algorithm based on the DMD reconstruction of the solution introduces small oscillations in the solution to (3.4). This is expected in such hyperbolic problems since the decay of the singular values of the dataset is very slow and the initial condition is non-smooth. However, such oscillations do not have an effect in the reconstruction of the flow.

To further validate our approach we compute the numerical error of the proposed algorithm. Since the results obtained with the global algorithm (2.9) with the Euclidean distance as cost function are the least accurate, we focus only on the other two approaches. Let us denote by  $\mathbf{X}_E^*$  and  $\tilde{\mathbf{X}}_E^*$  the matrices whose columns  $\mathbf{x}_E^*(t)$  and  $\tilde{\mathbf{x}}_E^*(t)$  are the solutions to the LP problems (2.9) and (3.2) respectively at time  $t$ , when the known terms  $\mathbf{b}(t) = \tilde{\mathbf{b}}(t)$  are chosen as the exact solution to (3.4) at time  $t$ . Analogously, let us denote by  $\mathbf{X}_D^*$  and  $\tilde{\mathbf{X}}_D^*$  the same matrices of solution when the known terms are obtained with the DMD method. We define the errors

$$E^G := \frac{\|\mathbf{X}_E^* - \mathbf{X}_D^*\|}{\|\mathbf{X}_E^*\|}, \quad E^L := \frac{\|\tilde{\mathbf{X}}_E^* - \tilde{\mathbf{X}}_D^*\|}{\|\tilde{\mathbf{X}}_E^*\|}, \quad (3.6)$$

where  $\|\cdot\|$  is the Frobenius norm. In Table 1 we compare the errors defined in (3.6) obtained from the simulations on a grid with  $N \times N$  nodes, for  $N = 20, 30$  and 40. As we can see from the table, increasing the number of nodes, we obtain the decrease of the error between the exact solution and the DMD reconstruction. Moreover, the error obtained with the local algorithm is significantly smaller than the one obtained with the global approach.

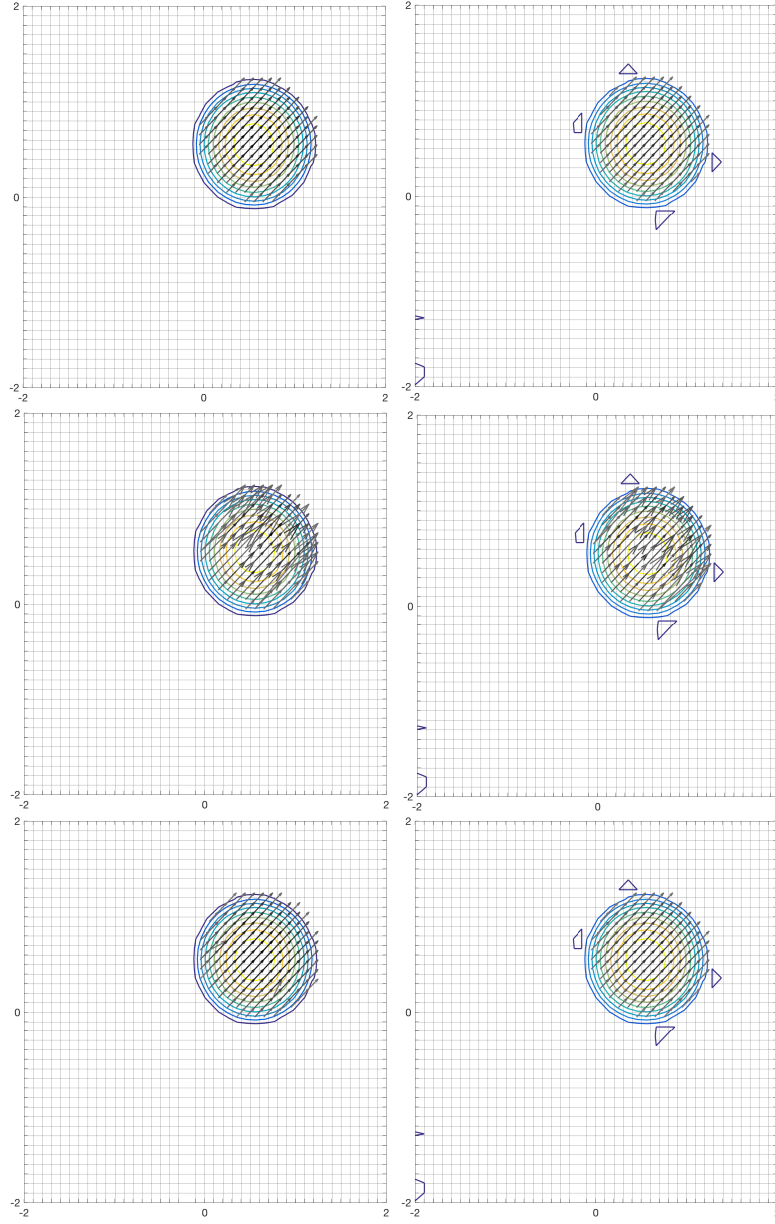


Figure 5: Reconstructed flows between  $t_1 = 0.725$  and  $t_2 = t_1 + \delta t$  superimposed to the level sets of the solution to (3.4) at  $t_2$ . Top row: local algorithm. Central row: global algorithm with  $c$  equal to the Euclidean distance. Bottom row: global algorithm with  $c$  defined in (3.5). Left column: the exact solution to (3.4) is used for computation. Right column: the DMD reconstruction of the solution to (3.4) is used for computation.

Table 1: Comparison of the errors defined in 3.6.

<b>Grid nodes</b>	$E^G$	$E^L$
20	0.42	0.053
30	0.40	0.05
40	0.33	0.04

Finally, in Table 2 we compare the computational time between the global approach (2.9), with the cost function as in (3.5), and the local approach (3.2).

Table 2: Computational time.

<b>Nodes</b>	<b>Global Exact</b>	<b>Global DMD</b>	<b>Local Exact</b>	<b>Local DMD</b>
20	17 sec	17.46 sec	0.17 sec	0.18 sec
30	11 min	11 min	0.47 sec	0.75 sec
40	2 h 50 min	2 h 50 min	1.25 sec	2.13 sec

#### 4. Application to real mobile phone data

In this section we focus on a specific application of the proposed approach. The real dataset gives information about the spatial distribution of people in a large populated area. The goal is to understand the travel flows of people, focusing in particular on recurring patterns and daily flows of commuters.

##### 4.1. Dataset

The Italian telecommunication company TIM provides estimates of mobile phones presence in a given area in raster form: the area under analysis is split into a number of elementary territory units (ETUs) of the same size (about  $130 \times 140 \text{ m}^2$  in urban areas). The estimation algorithm does not singularly recognize users and does not track them using GPS. It simply counts the number of phone attached to network nodes and, knowing the location and radio coverage

of the nodes, estimates the number of TIM users within each ETU at any time. TIM has now a market share of 30% with about 29.4 million mobile lines in Italy (AGCOM, Osservatorio sulle comunicazioni 2/2017).

The data we considered refer to the area of the province of Milan (Italy), which is divided in 198,779 ETUs, distributed in a rectangular grid  $389 \times 511$ . Data span six months (February, March and April 2016 and 2017). The entire period is divided into time intervals of 15 minutes, therefore we have 96 data per day per ETU in total. In Fig. 6 we graphically represent presence data at a fixed time. We observe that the peak of presence is located in correspondence of Milan city area. Fig. 7 shows the presences in the province of Milan in a typical

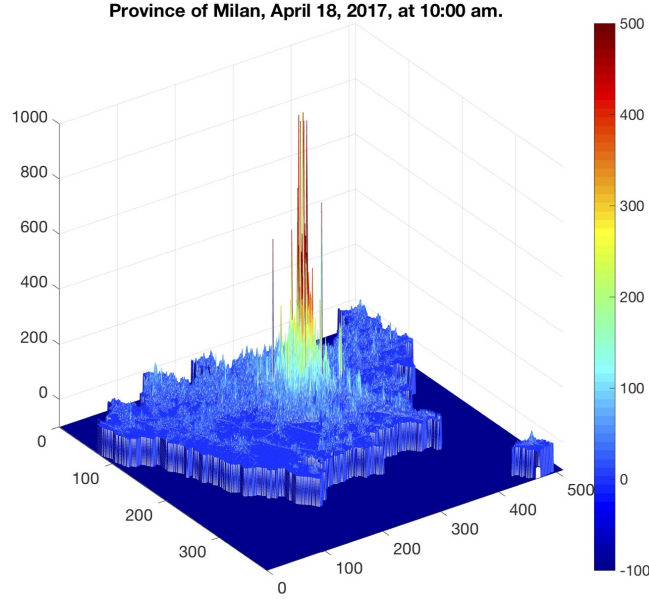


Figure 6: 3D-plot of the number of TIM users in each ETU of Milan's province on April 18, 2017.

working day in the left panel. The curve in the image decreases during the night, it increases in the day-time and decreases again in the evening. These variations are due to two main reasons: first, the arrival to and departure from Milan's province of visitors and commuters. Second, the fact that when a mobile phone

is switched off or is not communicating for more than six hours, its localization is lost. The presence value that most represents the population of the province is observed around 9 pm., when an equilibrium between traveling and phone usage is reached. This value changes between working days and weekends, but it is always in the order of  $1.3 \times 10^6$ . On the right panel of Fig. 7 we show the trend

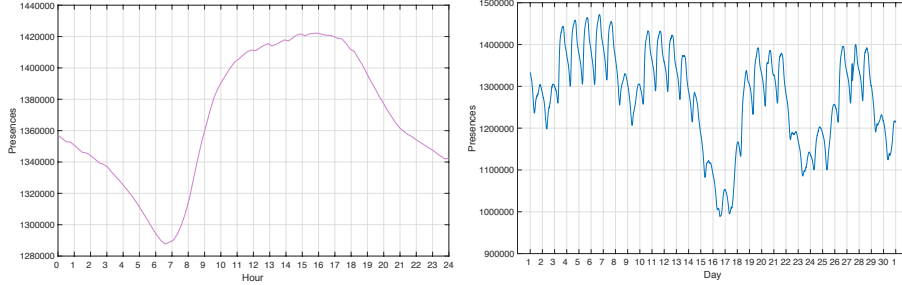


Figure 7: Trend of presences in the province of Milan during a typical working day (left). Trend of presences in the province of Milan during April 2017 (right).

of presence data during April 2017. We can observe a cyclical behavior: in the working days the number of presences in the province is significantly higher than during the weekends. It is interesting to note the presence of two low-density periods on April 15-18 and on April 22-26, 2017, determined respectively by the Easter and the long weekend for the Italy's Liberation Day holiday.

#### 4.2. DMD approach on TIM data

As explained in Section 2.1, we can reconstruct the presence data in each cell at any time. We denote by  $\mathbf{m}(t^i) \in \mathbb{R}^N$  the vector containing the number of people present in the  $N$  cells of the graph  $\mathcal{G}$  at a certain quarter of an hour and by  $\mathbf{m}(t^i + 15 \text{ min}) \in \mathbb{R}^N$  the same quantities at the consecutive time step. Applying the DMD method we are able to calculate  $\mathbf{m}(t) \in \mathbb{R}^N$  for any  $t \in [t^i, t^i + 15 \text{ min}]$ , see (2.2). We also note that DMD can be applied to higher dimensional dataset through randomized methods as explained in [1].

To validate the DMD approach on the TIM dataset we compute the relative Frobenius error between a whole day of real data and the DMD reconstruction.



Starting from the real data of presences every 15 minutes,  $\mathbf{P}^{data}$ , we reconstruct the data of presences every minute with the DMD algorithm,  $\mathbf{P}^{DMD}$ . Since a day contains 96 quarters of an hour and 1440 minutes,  $\mathbf{P}^{data}$  is a matrix  $96 \times N$ , while  $\mathbf{P}^{DMD}$  is a matrix  $1440 \times N$ . To compare the real data with the DMD reconstruction, we extract from  $\mathbf{P}^{DMD}$  the rows corresponding to the original intervals of 15 minutes into the matrix  $\tilde{\mathbf{P}}^{DMD}$ , of dimensions  $96 \times N$ , and then we define the error as:

$$E = \frac{\|\mathbf{P}^{data} - \tilde{\mathbf{P}}^{DMD}\|_F}{\|\mathbf{P}^{data}\|_F}, \quad (4.1)$$

where  $\|\cdot\|_F$  is the Frobenius norm. In Figure 8 we analyse a month of data in the whole area of the province of Milan. We can see the DMD is very accurate with a global error of order  $10^{-3}$  which certify the accuracy of the method.

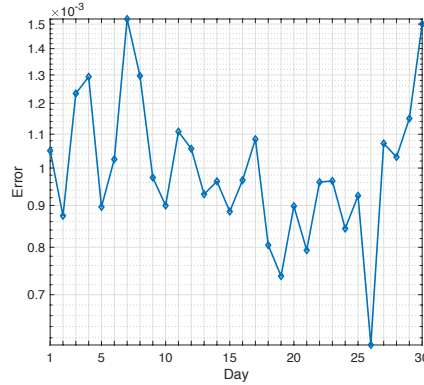


Figure 8: Global error defined in (4.1) where DMD has been computed with  $r = 95$  in step 2 of *Algorithm 1*.

#### 4.3. Understanding human mobility flows

Following the approach described in Section 3, we define the graph  $\mathcal{G}$  by exploiting the subdivision of the area of the province of Milan (Italy) into ETUs; we identify the  $N$  nodes of the graph with the corresponding center of the ETUs, ordered from the left to the right and from the top to the bottom. The result is a rectangular graph  $\mathcal{G}$  divided into  $N_R$  rows and  $N_C$  columns ( $N = N_R \times N_C$ ).

The mass  $m_j(t_n)$  is defined as the average number of presences in the node  $j$  at time  $t_n = n$  15 min.

Let us assume that  $V_{\max}$  in (3.1) is equal to 50 km/h. Since the dimensions of the ETUs is around 150 m, to apply the DMD we fix the new time step  $\delta t$  equal to 10 seconds. With this choice we assume that people can move only towards the eight adjacent nodes of the rectangular graph, or not move at all. We observe that the mass in the nodes on the four corners of the graph can move only towards four directions (adjacent nodes or no movement), while that on the boundaries can move only towards six directions. In this way, the total number of possible movements between the cells is given by

$$\tilde{N} = \underbrace{4 \cdot 4}_{\text{corners}} + \underbrace{6 \cdot 2 (N_R + N_C - 4)}_{\text{boundaries}} + \underbrace{9 (N - 4 - 2 (N_R + N_C - 4))}_{\text{internal nodes}} < 9N. \quad (4.2)$$

The vectors  $\tilde{\mathbf{x}}$  and  $\tilde{\mathbf{c}}$  associated to the unknown moving mass and to the cost function have length  $\tilde{N}$ , while the matrix  $\tilde{\mathbf{M}}$  of the LP problem (3.2) has dimension  $2N \times \tilde{N}$ . In Table 3, we compare the dimensions of the vectors and the matrices of the two different LP problems: it is clear that the computational time to solve problem (3.2) is significantly reduced respect to problem (2.9).

Table 3: Comparison between dimensions of matrix and vectors for the two methods.

Algorithm	Vectors Dimension	Matrix Dimension
Global	$N^2$	$2N^3$
Local	$\tilde{N} (< 9N)$	$2N \times \tilde{N} (< 18N^2)$

*Choice of the cost function  $c$ .* Since the ETUs are rectangles of length  $\ell_x = 130$  m and  $\ell_y = 140$  m, we define the cost function  $c_{jk}$  for the local algorithm as

follows:

$$c_{jk} = \begin{cases} 0 & \text{if } j = k \text{ or } j \text{ and } k \text{ are not adjacent} \\ \ell_x & \text{if } j \text{ and } k \text{ are horizontally adjacent} \\ \ell_y & \text{if } j \text{ and } k \text{ are vertically adjacent} \\ \sqrt{\ell_x^2 + \ell_y^2} & \text{if } j \text{ and } k \text{ are diagonally adjacent.} \end{cases}$$

For the global approach, we use the cost function defined in (3.5) with  $\varepsilon = 0.1$ .

To sum up, in order to solve the mass transfer problem for a whole day using snapshots taken every 15 minutes (real data) we have to solve 96 global LP-problems (2.9), whereas with the DMD algorithm we have to solve 8640 local LP-problems (3.2). As we will see in the following section, despite the larger number of LP problems, the local approach is more convenient than the global one.

#### 4.4. Numerical results

In this section we show the results obtained with the local algorithm (3.2) to study the flows of commuters and the influence of great events on human mobility. The flows are represented by arrows; we draw only those which correspond to the most significant movements, and we associate a darker color to the arrows corresponding to a larger movement of people.

##### 4.4.1. Flows of commuters

In the following simulations we consider the area of the Province of Milan during a generic working day. Milan is one of the biggest Italian city and it attracts many workers from outside. The city of Milan is located in the right part of the Province, therefore we mainly see movements from/to the left part of the analyzed area. In the top panel of Figure 9 we show the morning flows of a working day: we clearly see that the arrows are directed towards the city of Milan. In particular, we zoom on the arrows which overlap the roads heading to Milan. In the bottom panel of Figure 9 we show the opposite phenomenon: in the evening people go away from work to come back home inside the Province of Milan.

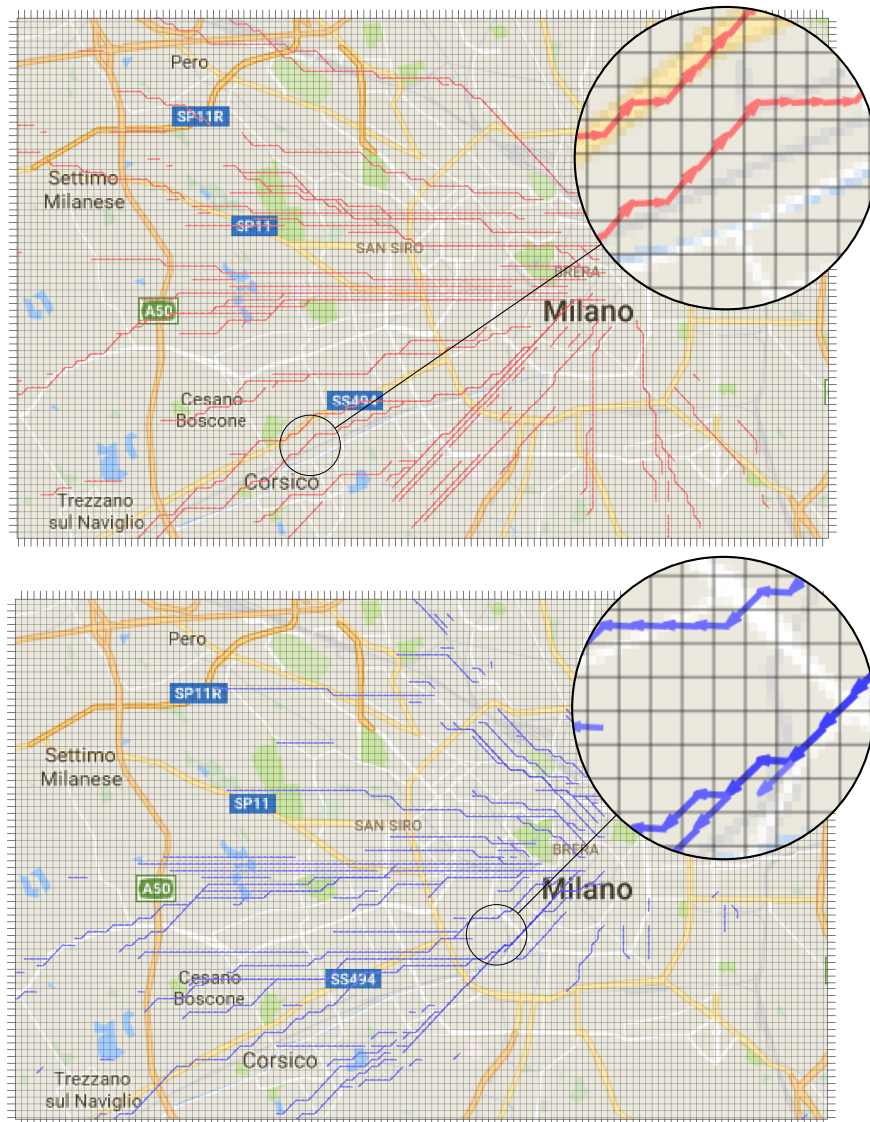


Figure 9: Top: Flows of commuters during the morning of a generic working day. Bottom: Flows of commuters during the evening of a generic working day.

*CPU times.* We consider data for a 6 hours frame on an area of  $144 \times 240$  cells the local algorithm requires 144 hours of CPU time. With the global approach (2.9) we are not able to analyze such an area, since the matrix  $\mathbf{M}$  in (2.9) has a computationally unmanageable dimension.

#### 4.4.2. Flows influenced by a great event

In this test we show how the algorithm is able to capture the way a big event influences human flows. The event we have considered is the exhibition of the *Salone del Mobile*, held every April at Fiera Milano exhibition center in Rho, near Milan. We analyze a square area of  $31 \times 31$  centered around Fiera Milano. In the left panel of Figure 10 we show the morning fluxes directed to the exhibition area whereas in the right panel we show the evening flows directed from the exhibition area to the outside.

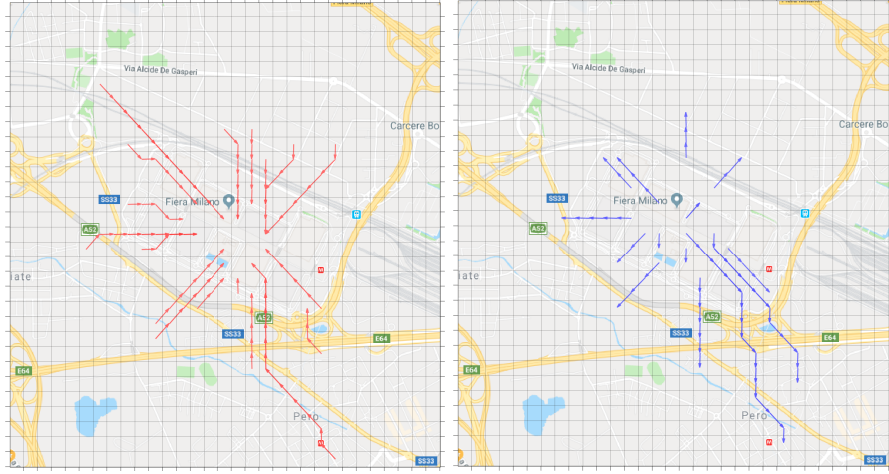


Figure 10: Main flows directed to the exhibition area in the morning (09:45 - 09:46) (left), Main flows from the exhibition area in the evening (18:00 - 18:01).(right)

*CPU times.* For a simulation of 18 hours, from 06:00 to 23:45, on an area of  $31 \times 31$  cells, the local algorithm requires 6 minutes of CPU time while the global approach requires 30 minutes.

## 5. Conclusions

In this paper we have proposed an efficient method to solve an inverse mass transfer problem, consisting in recovering the dynamics underlying the mass displacement. The proposed algorithm prevents to handle large displacements of the mass, thus saving CPU time and memory allocation with respect to other recently proposed solutions.

The application of the methodology to a real dataset describing the movement of people was also investigated. It is useful to note here that the applicability of the Wasserstein-based methodology was not at all obvious, since it is based on assumptions which are not totally fulfilled. Indeed, the choice of the cost function  $c$  does not take into account the fact that people move mainly along roads, are stopped by obstacles, buildings, etc., and in general are not free to move in all directions. Moreover, and most important, the computation of the Wasserstein distance stems from a global optimization problem in which the mass is considered as a whole. In other words, the optimal transport map  $T^*$  is found by minimizing the cost of the displacement of the whole crowd, without any distinction among people, and with no regards about individual targets. Despite this, the results we have obtained (see especially those in Figs. 9-10) are exactly as one can expect, meaning that the method is, overall, robust enough to work well even if the constitutive assumptions are not totally fulfilled.

## References

- [1] A. Alla and J.N. Kutz. Randomized model order reduction. *Advances in Computational Mathematics*, <https://doi.org/10.1007/s10444-018-09655-9>, 2019.
- [2] C. Balzotti, A. Bragagnini, M. Briani, and E. Cristiani. Understanding Human Mobility Flow from Aggregated Mobile Phone Data. In IFAC-

PapersOnLine, editor, *15th IFAC Symposium on Control in Transportation Systems CTS 2018*, volume 51-9, pages 25–30, 2018.

- [3] D.A. Bistrian and I.M. Navon. An improved algorithm for the shallow water equations model reduction: Dynamic Mode Decomposition vs POD. *International Journal for Numerical Methods in Fluids*, 78:552 – 580, 2015.
- [4] M. Briani, E. Cristiani, and E. Iacomini. Sensitivity analysis of the LWR model for traffic forecast on large networks using Wasserstein distance. *Commun. Math. Sci.*, 16(1):123–144, 2018.
- [5] P. Héas and C. Herzet. Optimal kernel-based Dynamic Mode Decomposition. <https://arxiv.org/pdf/1710.10919.pdf>.
- [6] P. Héas and C. Herzet. Optimal low-rank Dynamic Mode Decomposition. <https://arxiv.org/pdf/1701.01064.pdf>.
- [7] F. L. Hitchcock. The distribution of a product from several sources to numerous localities. *Studies in Applied Mathematics*, 20(1-4):224–230, 1941.
- [8] I.T. Jolliffe. *Principal component analysis*. Springer, 2002.
- [9] K. Pearson. On lines and planes of closest fit to systems of points in space. *Philosophical Magazine*, 2:559 – 572, 1901.
- [10] A. Quarteroni and A. Valli. *Numerical Approximation of Partial Differential Equations*. Springer, 1994.
- [11] F. Santambrogio. *Optimal transport for applied mathematicians*, volume 87 of *Progress in Nonlinear Differential Equations and their Applications*. Birkhäuser/Springer, Cham, 2015. Calculus of variations, PDEs, and modeling.
- [12] P. J. Schmid. Dynamic mode decomposition of numerical and experimental data. *Journal of Fluid Mechanics*, 656:5–28, 2010.

- [13] S.M. Sinha. *Mathematical Programming: Theory and Methods*. Elsevier, 2005.
- [14] G. Tissot, L. Cordier, N. Benard, and B.R. Noack. Model reduction using dynamic mode decomposition. *Comptes Rendus Mécanique*, 342:410–416, 2014.
- [15] J.H. Tu, C.W. Rowley, D.M. Luchtenburg, S.L. Brunton, and J.N. Kutz. On dynamic mode decomposition: Theory and applications. *AIMS*, 1:391–321, 2014.
- [16] C. Villani. *Optimal transport: old and new*, volume 338. Springer Science & Business Media, 2008.
- [17] S. Volkwein. *Model Reduction using Proper Orthogonal Decomposition*. Lecture notes, University of Konstanz, 2011.
- [18] D. Zhu, Z. Huang, L. Shi, L. Wu, and Y. Liu. Inferring spatial interaction patterns from sequential snapshots of spatial distributions. *International Journal of Geographical Information Science*, 32(4):783–805, 2018.